AMERICAN SOCIETY FOR MICROBIOLOGY | Microbiology Spectrum

RESEARCH ARTICLE

Phosphomannose Isomerase Is Involved in Development, Stress Responses, and Pathogenicity of *Aspergillus flavus*

Sayed Usman,[a,b] Chao Du,[a,b] Qijian Qin,[b] Arome Solomon Odiba,[b,c] Rui He,[a,b] Bin Wang,[b] Cheng Jin,[a,b,c] Wenxia Fang[a,b]

[a]College of Life Science and Technology, Guangxi University, Nanning, Guangxi, China
[b]Guangxi Biological Sciences and Biotechnology Center, Guangxi Academy of Sciences, Nanning, Guangxi, China
[c]State Key Laboratory of Mycology, Institute of Microbiology, Chinese Academy of Sciences, Beijing, China

Sayed Usman and Chao Du contributed equally to this work. Author order was determined based on who took the lead in writing the manuscript.

ABSTRACT *Aspergillus flavus* causes invasive aspergillosis in immunocompromised patients and severe contamination of agriculturally important crops by producing aflatoxins. The fungal cell wall is absent in animals and is structurally different from that of plants, which makes it a potential antifungal drug target due to its essentiality for fungal survival. Mannose is one of the important components in the fungal cell wall, which requires GDP-mannose (GDP-Man) as the primary donor. Three consecutive enzymes, namely, phosphomannose isomerase (PMI), phosphomannose mutase (PMM), and GDP-mannose phosphorylase (GMPP), are required for GDP-Man biosynthesis. Thus, PMI is of prime importance in cell wall biosynthesis and also has an active role in sugar metabolism. Here, we investigated the functional role of PMI in *A. flavus* by generating a *pmiA*-deficient strain. The mutant required exogenous mannose to survive and exhibited reduced growth rate, impaired conidiation, early germination, disturbance in stress responses, and defects in colonization of crop seeds. Furthermore, attenuated virulence of the mutant was documented in both *Caenorhabditis elegans* and *Galleria mellonella* infection models. Our results suggested that PMI plays an important role in the development, stress responses, and pathogenicity of *A. flavus* and therefore could serve as a potential target for battling against infection and controlling aflatoxin contamination caused by *A. flavus*.

IMPORTANCE *Aspergillus flavus* is a common fungal pathogen of humans, animals, and agriculturally important crops. It causes invasive aspergillosis in humans and also produces highly carcinogenic mycotoxins in postharvest crops that threaten food safety worldwide. To alleviate or eliminate the threats posed by *A. flavus*, it is necessary to identify genes involved in pathogenicity and mycotoxin contamination. However, little progress has been made in this regard. Here, we focused on PMI, which is the first enzyme involved in the biosynthesis pathway of GDP-Man and thus is important for cell wall synthesis and protein glycosylation. Our study revealed that PMI is important for growth of *A. flavus*. It is also involved in conidiation, germination, morphogenesis, stress responses, and pathogenicity of *A. flavus*. Thus, PMI is a potent antifungal target to curb the threats posed by *A. flavus*.

KEYWORDS *Aspergillus flavus*, drug target, pathogenicity, phosphomannose isomerase, stress response

Aspergillus flavus is one of the most common fungal pathogens of animals, plants, and humans. Being the second-most causative agent for invasive aspergillosis, *A. flavus* is associated with a high mortality rate, just after *Aspergillus fumigatus* (1, 2). During the current pandemic, COVID-19 patients have been investigated with complications of aspergillosis caused by *A. flavus* (3, 4). The fungus is also capable of infecting economically important crops like maize, peanut, corn, and cotton (5) and producing highly carcinogenic aflatoxins (AFs), which pose severe threats to human and animal health (6). It is of a dire need to develop

Editor Robert A. Arkowitz, Université Côte d'Azur, CNRS, Inserm

Address correspondence to Wenxia Fang, wfang@gxas.cn, or Cheng Jin, jinc@im.ac.cn.

The authors declare no conflict of interest.

Received 21 July 2022
Accepted 31 July 2022
Published 18 August 2022

new approaches and drug targets involved in pathogenicity and mycotoxin production to curb the serious threats posed by *A. flavus* (7).

The fungal cell wall is an important organelle providing protection to the cell, maintaining cellular integrity and proper homeostasis (8–10). Since the fungal cell wall is absent in animal cells and different from the plant cell wall, it is considered a promising target for developing antifungal drugs (11). Glucans, chitin, mannan, and glycoproteins are the main components of the fungal cell wall (12). UDP-glucose (UDP-Glc), UDP-GlcNAc, and GDP-Man are the three precursors required for cell wall biosynthesis (13). Previously, enzymes involved in the UDP-GlcNAc pathway such as GNA1, AGM1, and UAP1 have been identified as potential drug targets against *A. fumigatus* (14–16). Phosphomannose isomerase (PMI), phosphomannose mutase (PMM), and GDP-Man pyrophosphorylase (GMPP) are the three crucial enzymes involved in the biosynthesis of GDP-Man, which is required for cell wall mannan biosynthesis and protein glycosylation (17).

As the first committed enzyme in the GDP-Man pathway, PMI catalyzes the conversion between fructose-6-phosphate (Fru6P) and mannose-6-phosphate (Man6P), thus linking glycolysis to the GDP-Man pathway (18). This enzyme is present in mammals, bacteria, and fungi and plays an important role in cell wall synthesis, viability, and cell signaling (19). Depletion of PMI in eukaryotes results in Man6P accumulation, which leads to toxicity and glycosylation defects (20). Until now, the functional role of PMI has been reported in many organisms such as *A. fumigatus*, *Cryptococcus neoformans*, *Leishmania mexicana*, and *Metharizum acridum* (17, 21–23). The PMI deletion mutant of *A. fumigatus* is unable to grow without the supplementation of external mannose in the growth medium. The mutant exhibited defects in cell wall integrity, abnormal morphology, and reduced conidiation (21). Similarly, the *C. neoformans* PMI-disrupted mutant exhibits complete avirulence, poor capsule formation, and morphological abnormalities (17). Compared with the wild type, the *L. mexicana* Δ*pmi* mutant exhibits attenuated virulence and was deficient in glycoconjugates synthesis, although it is able to grow in the absence of exogenous mannose (22). In the entomopathogenic fungus *M. acridum*, the PMI-deficient strain exhibited less virulence and also showed increased sensitivity to cell stress conditions (23). All these studies demonstrate that PMI plays a central role in development, cell wall synthesis, and virulence.

In the present study, we constructed a PMI-deficient strain of *A. flavus* and investigated the biological role of PMI. Our results indicated that PMI-deficient strain in *A. flavus* required exogenous mannose for growth. Furthermore, PMI contributed to the development, stress responses, colonization of crops, and pathogenicity of *A. flavus* and thus is a potential drug target for controlling the threats caused by *A. flavus*.

RESULTS

Construction of PMI deletion mutant in *A. flavus*. Performing a tBLASTn search with *A. fumigatus* PMI (UniProt accession no. Q66WM4) revealed one *pmiA* gene in the *A. flavus* genome with an open reading frame (ORF) of 1,386 bp, encoding a protein of 461 amino acids (UniProt accession no. B8N4V5). A phylogenetic tree constructed using protein sequences revealed that *A. flavus* PMI shared 98% identity with *Aspergillus oryzae* and 35% identity with *Fusarium oxysporum* (see Fig. S1A in the supplemental material). To determine the role of PMI in *A. flavus*, the Δ*pmiA* mutant was constructed using homologous recombination strategy (Fig. S1B). Since *pmi* mutant of *A. fumigatus* requires exogenous mannose for growth (21), we used regeneration medium containing 3 mM mannose to facilitate *pmiA* mutant screening in *A. flavus*. The revertant strain (RT) was constructed by the insertion of *pmiA* back into the original gene locus under no mannose supplementation for screening; then, *pyrG* was inserted to replace the stop codon of the *pmiA*, thus making the RT strain autotrophic. The Δ*pmiA* and the RT strains were confirmed using four pairs of primers to ensure the correct recombination (Table S1 and Fig. S1C).

Δ*pmiA* requires exogenous mannose for growth. In *A. fumigatus*, the growth of the Δ*pmiA* mutant was different in the medium supplied with different amounts of mannose. Similarly, when grown on minimal medium (MM) with various mannose (Man) concentrations (0, 0.5, 3, 5, 10, and 25 mM), the optimum growth of the Δ*pmiA* mutant was observed at 3 mM, which was defined as MMM condition for subsequent phenotypic analysis. Mannose

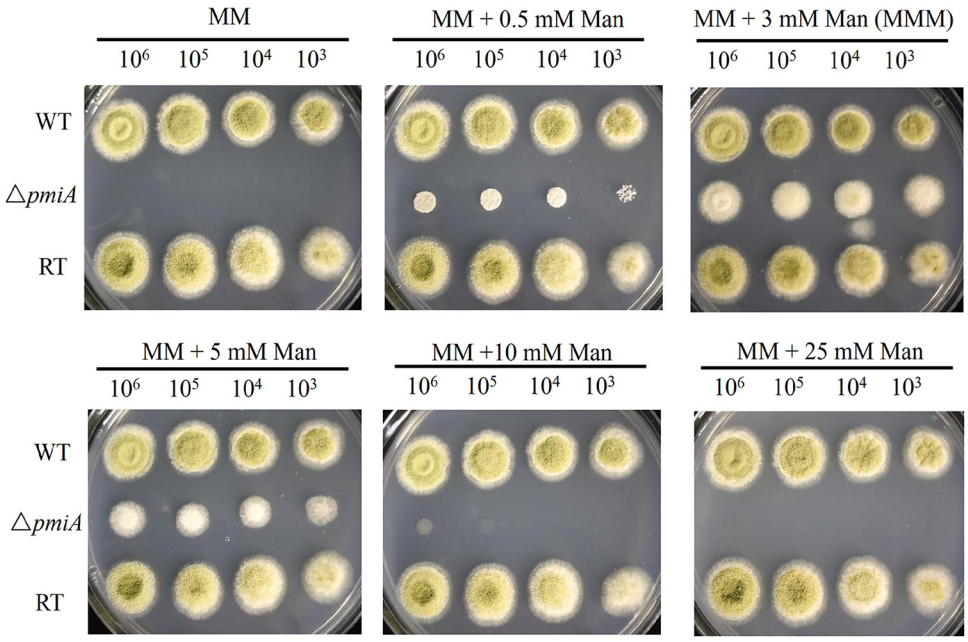

FIG 1 Growth of PMI mutants at different concentrations of mannose. Freshly harvested conidia of WT, Δ*pmiA*, and RT strains were serially diluted and spotted on MM media supplemented with 0, 0.5, 3, 5, 10, and 25 mM mannose. Plates were incubated at 37°C for 48 h.

at 0.5 and 5 mM only supported partial growth of the mutant, but over 10 mM mannose completely abolished the growth of the mutant, revealing that a large amount of mannose was not suitable for the mutant growth (Fig. 1). To further dissect this phenomenon, growth stages of the mutant in various concentrations of mannose were monitored under microscope. The Δ*pmiA* mutant displayed short ballooned germ tubes at 0.5 mM mannose, whereas longer germ tubes were seen at 3 mM and 5 mM, similar to the phenotype of the Δ*pmi1* mutant in *A. fumigatus* (21). Partial conidia started to germinate at 10 mM mannose after 10 h of incubation and produced ballooned hyphal tips after 48 h (Fig. S2). However, no conidia germinated at 25 mM and 40 mM mannose even after 48 h of incubation (Fig. S2). Since mannose will be phosphorylated into Man6P once it enters the cells, the above-described results implied that less than 3 mM mannose was not sufficient for the GDP-Man pathway in the mutant; higher than that amount probably led to excess Man6P accumulated due to the PMI deficiency, as well as accompanied ATP depletion for the phosphorylation process, thus keeping the conidia at the resting stage. In contrast, the wild-type (WT) and RT strains grew well irrespective of the exogenous mannose amount, indicating that apart from supplying sufficient Man6P for the GDP-Man biosynthesis pathway, the rest of the Man6P would be converted to Fru6P by PMI for energy production. Furthermore, the mutant was unable to grow on sole carbon sources, including sucrose, xylose, maltose, glycerol, galactose, mannose, GlcN, GlcNAc, and arabinose, except fructose, which only supported limited growth (Fig. S3). However, when we supplemented different concentrations of fructose (Fru) into MM containing 1% glucose, the mutant was unable to grow in all tested conditions, whereas the WT and RT strains grew well (Fig. S4). These results suggest that *A. flavus* PMI is important for growth and survival.

Deletion of *pmi* led to reduced conidiation and abnormal morphogenesis. Since MMM is the optimum condition for the *A. flavus* Δ*pmiA* mutant, we further characterized its growth in more detail. When conidia of the WT, Δ*pmiA*, and RT strains were spotted on MMM, the mutant colony was less yellow than the WT and RT strains (Fig. 2A). No significant differences in the colony diameter were observed at the first 4 days, but the mutant displayed a smaller colony afterward (Fig. 2B). After 10 days of incubation, conidial counting showed that deletion of *pmiA* significantly reduced conidiation. Compared with that of the WT and RT, conidia produced by the mutant were decreased by 233- and 176-fold, respectively (Fig. 2C). To unravel the reason for the reduced conidiation in the mutant, lactic acid

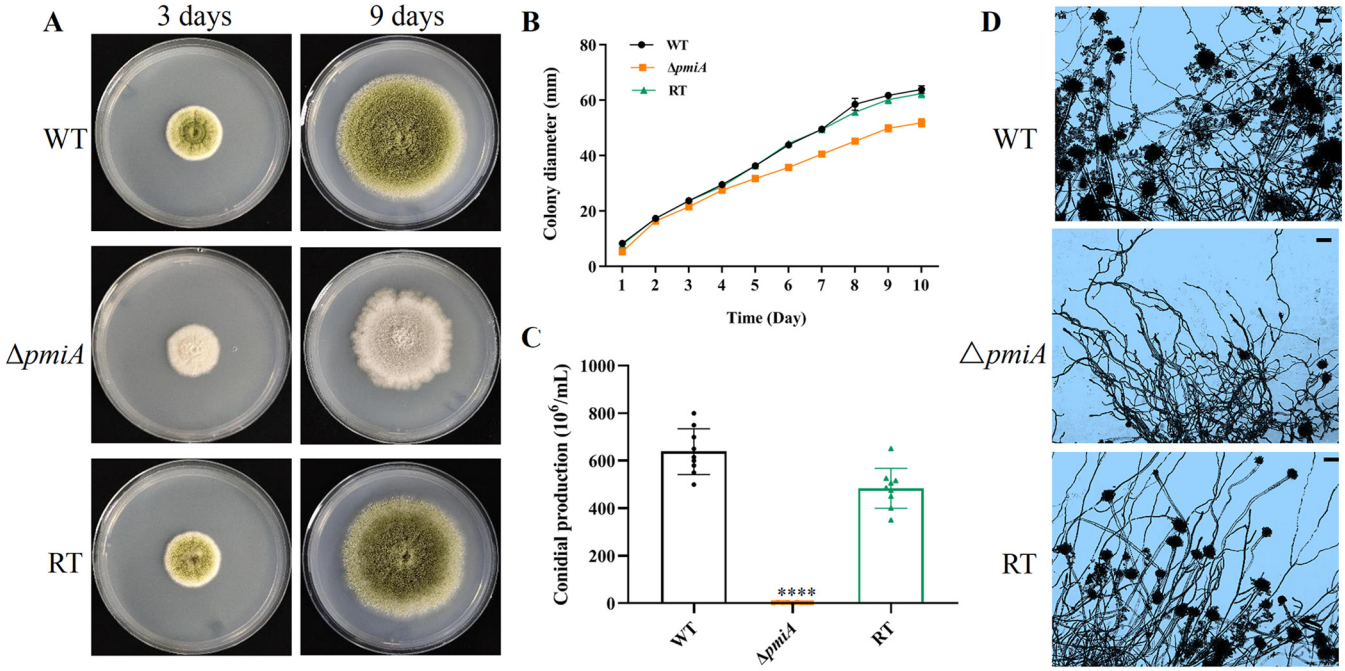

FIG 2 Growth of the WT, Δ*pmiA*, and RT strains on MMM. (A) Conidia of the WT, Δ*pmiA*, and RT strains were inoculated on MMM and incubated at 37°C for 3 and 9 days. (B) Colony diameter was recorded daily for 10 days for the three strains grown on MMM plates. Three replicates were performed, and data were shown as mean ± SD. (C) Conidia production was measured using a hemocytometer after 10 days of incubation on MMM at 37°C. Values represent the mean ± SD; multiple *t* test analysis was used to indicate statistical significance (****, $P < 0.0001$). (D) Conidiophore morphology of the WT, Δ*pmiA*, and RT was examined under a microscope after staining (scale bar represents 10 μm).

phenol cotton blue staining was applied and checked under a microscope. As shown in Fig. 2D, the conidiophores of the mutant were significantly less than those of the WT and RT strains, which explained the reduced conidial production.

In liquid MMM medium, the mutant conidia displayed faster germination, with nearly 40% of the conidia germinated at 6 h compared with 5% and 6% of the WT and RT, respectively. However, the germination rate of the mutant became slower at 8 h and 10 h than the WT and RT, and 14% of the mutant spores remained dormant even at 10 h (Table 1). Moreover, the hyphal morphology of the mutant was abnormal, including unorganized polarity or multibranches at 10 h (Fig. 3). Overall, PMI deficiency resulted in reduced conidiation, early germination, and abnormal morphogenesis in *A. flavus*.

***pmiA* deletion interrupted sclerotia formation and stress responses in *A. flavus*.** To overcome the stresses of the external environment, *A. flavus* often develops sclerotia, which act as repositories for the production of sexual spores (24). To evaluate the role of PMI in sclerotia formation, conidia of the WT, Δ*pmiA*, and RT strains were spotted in yeast extract-peptone-dextrose (YPD) medium with 3 mM mannose supplementation. After incubation at 37°C for 10 days, the spores were washed off with 75% ethanol. As shown in Fig. 4, the formation of sclerotia was severely impaired in the Δ*pmiA* mutant in contrast to that in the WT and RT, indicating that PMI might be involved in withstanding adverse environmental conditions. We next tested the responses of the mutant toward chemical and osmotic stresses.

TABLE 1 Germination rate of the Δ*pmiA* mutant in liquid MMM[a]

	Conidial germination rate (%) of:		
Time point (h)	WT	Δ*pmiA*	RT
6	5 ± 2	40 ± 6	6 ± 3
8	83 ± 4	81 ± 7	90 ± 1
10	94 ± 1	86 ± 1	96 ± 1

[a]Approximately 100 spores of each strain were captured for germination rate statistics. The experiments were repeated twice, and the data were presented as mean ± SD.

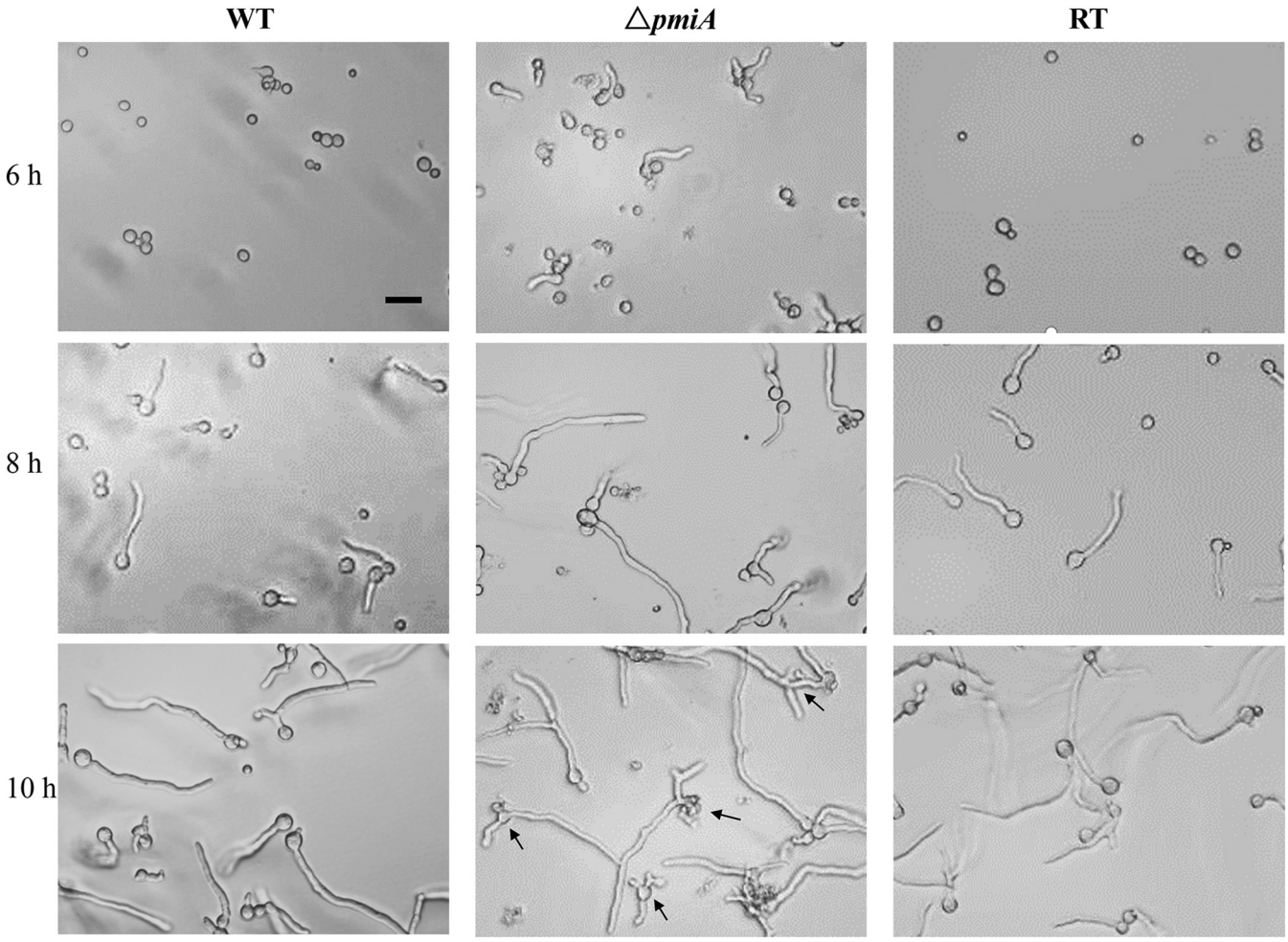

FIG 3 Germination morphology of the Δ*pmiA* mutant in liquid MMM. A differential interference contrast (DIC) microscope (Leica) was used to record the germination rates of the WT, Δ*pmiA*, and RT strains at 6 h, 8 h, and 10 h of cultivation at 37°C. Black arrows indicated abnormal morphology. Scale bar represents 10 μm.

The results indicated that the cell wall stressor Congo red (CR), cell membrane stressor sodium dodecyl sulfate (SDS), and the oxidative stressor H_2O_2 significantly inhibited the growth of the Δ*pmiA* mutant but not WT and RT strains (Fig. 5). We further quantified cell wall components by using a previously reported method (25). Our results demonstrated that the amounts of cell wall polysaccharides were not significantly changed in the Δ*pmiA* mutant compared with the WT and RT strains (Fig. S5). However, lack of PMI might contribute to defective mannosylation of cell wall proteins, leading to increased sensitivity to CR and SDS. It has been reported that osmotic stabilizers could rescue fungi conidiation (26). Unexpectedly, the mutant displayed supersusceptibility to all osmotic stabilizers, indicating that those osmotic stabilizers exert stresses on the mutant (Fig. 5). It is obvious that *pmi* deletion interrupted sclerotia formation and stress responses in *A. flavus*.

***pmi* deletion affected colonization in crop seeds.** Since the above-described results indicated that PMI affected growth, conidiation, and sclerotia formation in *A. flavus*, we therefore hypothesized that the pathogenicity of the Δ*pmiA* mutant might be deficient in plant seeds. To test the hypothesis, peanut and corn seeds were used for infection. After incubation at 28°C for 6 days in the dark, peanut and corn seeds were severely infected by the WT and RT, with a large number of conidia produced on the surface of the seeds, whereas the seeds infected by the mutant displayed no symptoms (Fig. 6A). The conidia washed from the seeds infected by the mutant were significantly less than those from the seeds infected by WT and RT (Fig. 6B and C). To further assess the cause of reduced pathogenicity of the Δ*pmiA* mutant, we tested the growth rate of the mutant on agar plates

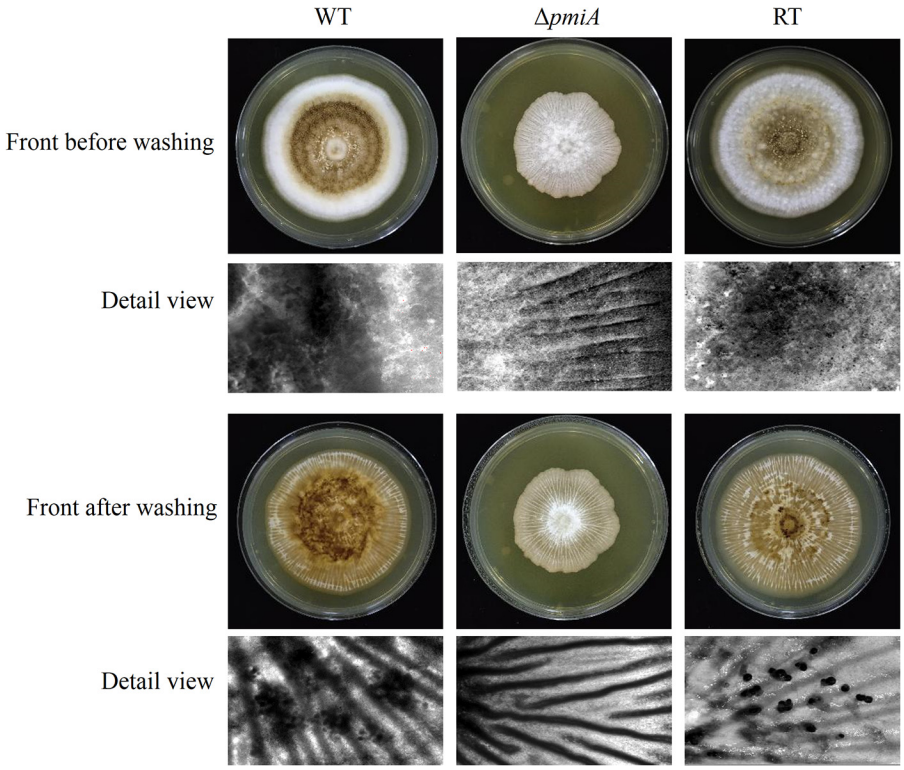

FIG 4 Sclerotia formation of the Δ*pmiA* mutant on YPD with 3 mM Man. Sclerotia production before and after washing with ethanol was viewed under a stereomicroscope after 10 days of incubation at 37°C in the dark.

supplemented with 1%, 3%, and 5% of peanut or corn powder as nutrients. As shown in Fig. S6, the mutant conidium was unable to germinate on those plates. Additionally, the mycelium of the mutant was also unable to grow on the above-described plates (Fig. S7), suggesting that the Δ*pmiA* mutant cannot utilize crop seed nutrients for growth.

We further analyzed the amount of aflatoxin B1 (AFB1) accumulated in the infected seeds. Thin-layer chromatography (TLC) analysis revealed that AFB1 was accumulated in the seeds infected by the WT and RT strains, whereas no AFB1 was detected in the seeds infected by the Δ*pmiA* mutant (Fig. 7). These results demonstrate that the Δ*pmiA* mutant loses its ability to colonize and grow on crop seeds, and AFB1 cannot be accumulated in the mutant infected crops.

Since the above-described plant infection studies were carried out at 28°C, we characterized the temperature effect on the growth of the mutant. As shown in Fig. S8A, in contrast to the WT and RT strains, the mutant displayed similar growth patterns at 28°C, 37°C, and 42°C. Furthermore, the mutant exhibited reduced conidiation and retarded growth rate at 28°C (Fig. S8B through D), similar to the performance at 37°C. When we used YPD plates supplemented with mannose for sclerotia production at 28°C, the WT and RT strains showed less sclerotial structures; therefore, the peanut powder plates (1%) were applied for the WT and RT strains. MMM medium was added to support the growth of mutant. After 7 days incubation in dark, both the WT and RT produced clear sclerotia, whereas no sclerotia were produced by the mutant (Fig. 8). Since PMIs are not important/essential in plants and are reported absent in many plants (27), it is promising that inhibitors targeting *A. flavus pmiA* will be applicable in the agricultural field, at least for prophylaxis of postharvest crop contamination.

PMI deficiency led to attenuated virulence in animal infection models. Since *A. flavus* is the second causative agent of aspergillosis and a serious threat to humans, we next investigated the pathogenicity of the Δ*pmiA* mutant in a *Caenorhabditis elegans* infection model (28). The survival rates of worms infected with the WT, mutant, and RT strains were counted at intervals of every 24 h and then plotted with Kaplan-Meier survival curves. As shown in Fig. 9A and Table S2A, the Δ*pmiA* mutant was found to be significantly less virulent than

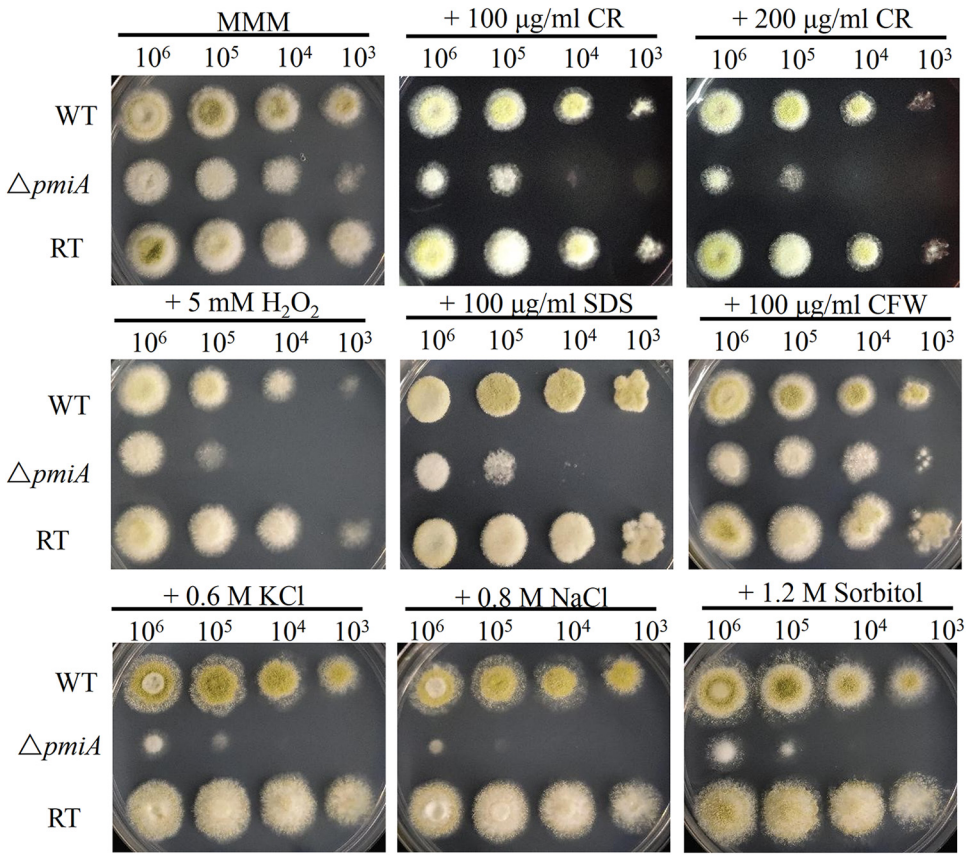

FIG 5 Responses of the Δ*pmiA* mutant to various stresses. We inoculated 10^6 to 10^3 serially diluted conidia on MMM supplemented with 100 μg/mL and 200 μg/mL CR, 5 mM H_2O_2, 100 μg/mL SDS, 100 μg/mL CFW, 0.6 M KCl, 0.8 M NaCl, and 1.2 M sorbitol. Plates were incubated at 37°C for 2 days.

the WT and RT strains. After 72 h of infection, the survival rates of the worms infected by the WT, mutant, and RT were 20%, 79%, and 19%, respectively. Since hyphal formation is critical for virulence (29), the hyphal filamentation rates in infected worms were also recorded. Similar to the virulence results, there was no hyphal filamentation in the Δ*pmiA* mutant, whereas the WT and RT-infected worms displayed 55% and 51% filamentation, respectively (Table S2A).

The pathogenicity was also evaluated in a *Galleria mellonella* infection model at 28°C, and a similar trend was observed as in the *C. elegans* model. The larvae infected with the Δ*pmiA* mutant and heat-killed conidia showed 73% and 80% survival rates, respectively, after 72 h of infection compared with those of the WT and RT strains (13% and 7%, respectively) (Fig. 9B and Table S2B). Collectively, these results indicate that PMI is involved in the pathogenicity of *A. flavus* in both *C. elegans* and *G. mellonella* infection models.

DISCUSSION

As an opportunistic fungal pathogen, *A. flavus* ranks second after *A. fumigatus* in causing deadly invasive aspergillosis (2, 30). Moreover, *A. flavus* is capable of producing aflatoxins in maize, groundnut, cassava, almond, peanuts, and many other important agricultural crops, which is a major concern for food safety (31–33). Among aflatoxins, AFB1 is highly carcinogenic and causes severe digestive, nervous, vascular, and estrogenic defects, thus posing threats to animals and humans (34, 35).

The fungal cell wall maintains the structure and integrity of the fungal cell (36) and thus is associated with physiology and essential biological processes (37). Since the fungal cell wall structure is unique to fungi, different from plants' cell walls and absent in human cells, it is proposed as a promising target for antifungal strategies (38). Mannose is an essential component for the synthesis of cell wall mannoproteins and mannan (13). As a primary

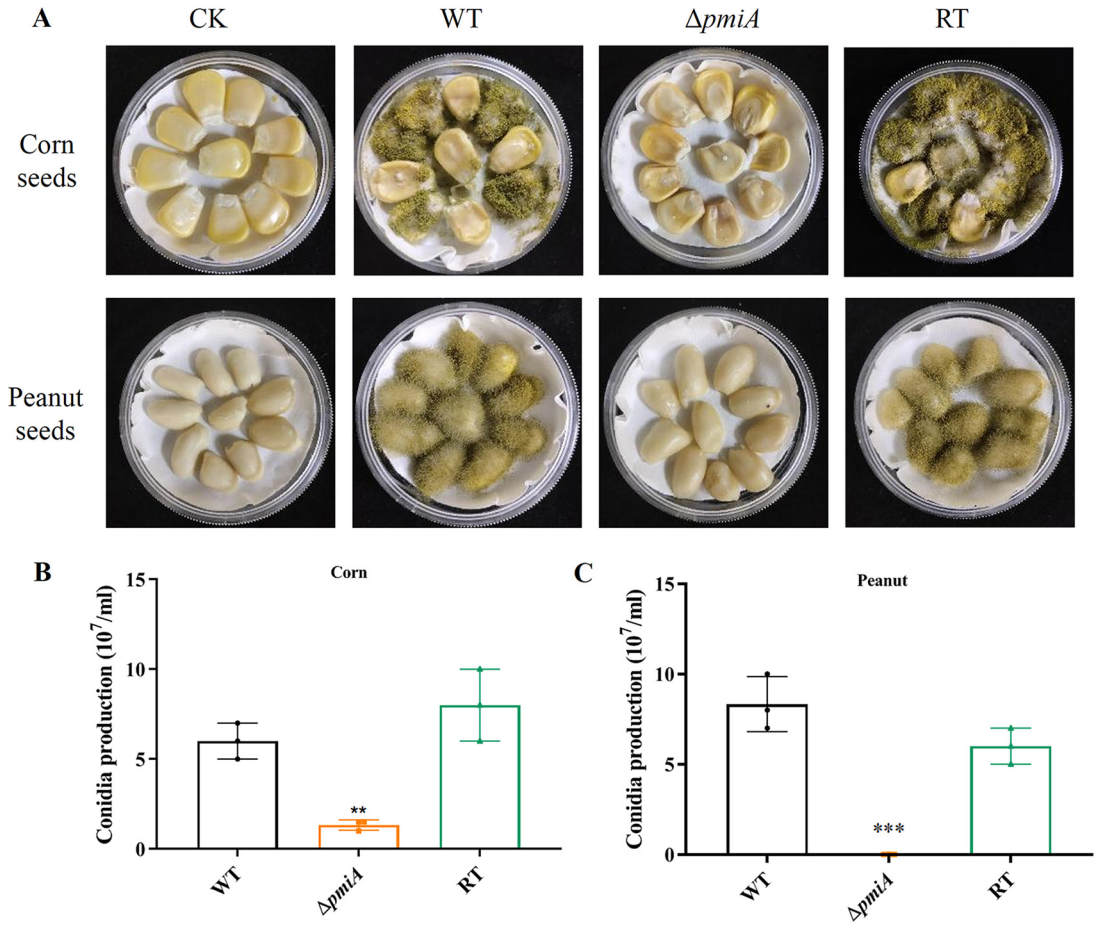

FIG 6 Colonization assay of *A. flavus* strains on crop seeds. (A) We inoculated 10^6 conidia from the WT, Δ*pmiA*, and RT strains on corn and peanut seeds, and the plates were incubated at 28°C for 6 days in the dark. (B) Conidia washed from infected peanut seeds were counted by hemocytometer. (C) Conidia washed from infected corn seeds were counted by hemocytometer. The experiment was conducted in three biological repeats.

mannose donor, GDP-Man is synthesized from Fru6P by three bioactive enzymes, PMI, PMM, and GMPP. Fru6P is also an important intermediate in glycolysis (39). The function of PMI has been characterized in *A. fumigatus*, revealing its essentiality for cell wall synthesis and morphogenesis (21). In the current study, the functional role of PMI in *A. flavus* was investigated by constructing a deletion mutant and conducting phenotypic analysis.

Similar to the *A. fumigatus* Δ*pmi* mutant, the PMI-deficient strain in *A. flavus* was unable to grow without the supplementation of exogenous mannose. Three millimolar mannose was sufficient for the optimal growth of the mutant whereas, higher concentrations of mannose (>10 mM) inhibited the growth of the mutant (Fig. 1 and see Fig. S2 in the supplemental material). On the other hand, the WT and RT grew well irrespective of exogenous mannose. These results indicate that PMI is required for balancing and buffering mannose metabolism in *A. flavus*. The high mannose inhibition on the germination and growth of the mutant was likely due to the phosphorylation and dephosphorylation of mannose accompanied by intracellular ATP depletion, just like the "honeybee effect" (40). We also noticed that fructose as the sole carbon source could restore partial growth of the mutant, whereas when it was added into MM in which glucose was the main carbon source, the mutant exhibited no growth at all (Fig. S3 and S4). Since the mutant required as little as 0.5 mM mannose to grow, we speculate mannose is an unavoidable impurity (<1%) during fructose production, thus supporting partial growth of the mutant when fructose was the sole carbon source. However,

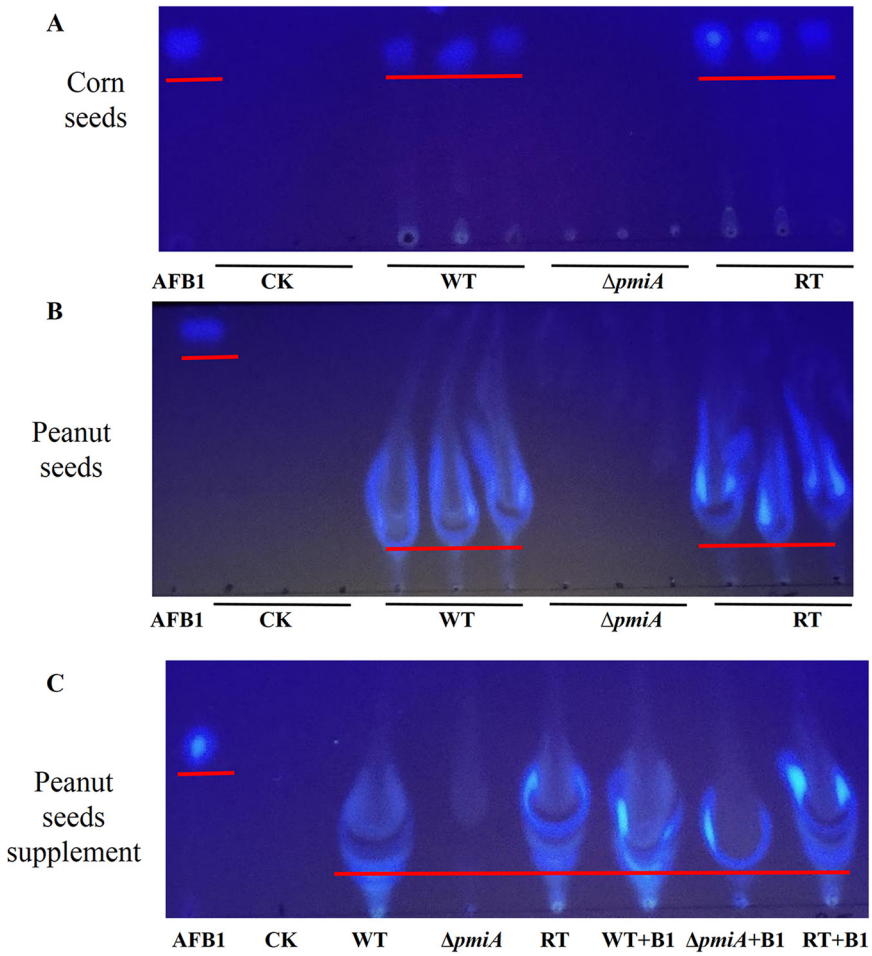

FIG 7 TLC analysis of AFB1 produced in infected seeds. Aflatoxin was extracted from conidia washed from infected peanut and corn seeds with an equal amount of chloroform. Chloroform was used as a control (CK). (A) Detection of AFB1 in corn seeds; (B) detection of AFB1 in peanut seeds; (C) verification of peanut oil interference on TLC. AFB1 standard was added into each sample for comparison.

when both glucose and fructose were supplied, the uptake of fructose (and its impurities) was blocked due to the carbon catabolite repression (41); therefore, the growth of the mutant could not be restored. Both small and large amounts of mannose severely impaired the germination of the Δ*pmiA* mutant in which low concentrations of mannose led to abnormal hyphal morphology, whereas high concentrations of mannose blocked the germination of the Δ*pmiA* mutant (Fig. 3 and Fig. S2).

PMM and GMPP in the GDP-Man biosynthesis pathway have been shown to have an impact on the development of *A. fumigatus*. It has been reported that PMM in *A. fumigatus* is indispensable for survival and its deletion leads to altered cell wall organization and certain morphological abnormalities such as reduced conidiation, abnormal polarity, retarded growth, and germination (42). Similarly, the GMPP conditional mutant of *A. fumigatus* exhibited phenotypic defects, including hyphal lysis, rapid germination, reduced conidiation, and altered cell wall integrity (43). Consistently, our study showed that *A. flavus* PMI was involved in growth, conidiation, and morphogenesis (Fig. 2 and 3). Despite that functions of PMIs in closely related *A. fumigatus* and *A. nidulans* have been studied previously, our work that focused on the *A. flavus* Δ*pmiA* mutant revealed different phenotypes, including faster germination, interrupted sclerotia formation, and supersusceptibility to osmotic stabilizers, which usually act for salvage competence in other fungal PMI mutants (21, 44).

Since PMI is the first committed enzyme in the GDP-Man biosynthesis pathway, we proposed that PMI deletion may have direct effects on the cell wall integrity. Indeed, the *A. flavus* Δ*pmiA* mutant was sensitive to CR, but cell wall polysaccharides of the mutant were

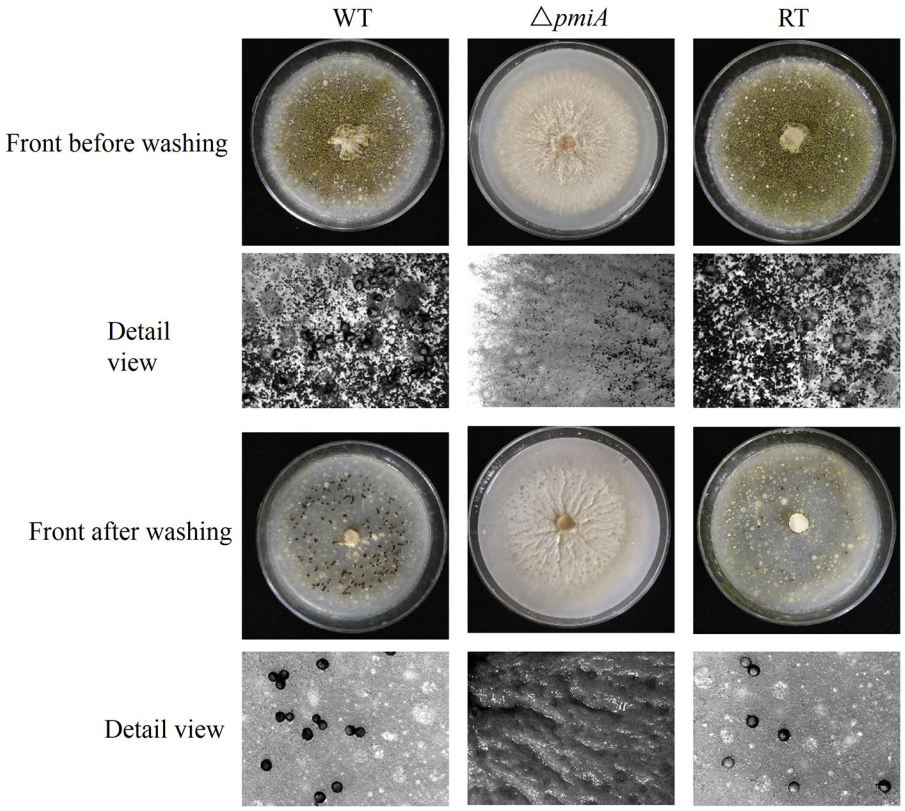

FIG 8 Sclerotia formation of the Δ*pmiA* mutant on MMM supplemented with 1% peanut powder. Sclerotia production before and after washing with ethanol was viewed under a stereomicroscope after 7 days of incubation at 28°C in dark. We applied 1% peanut powder plates for the WT and RT strains.

similar to those of the WT and RT strains (Fig. 5 and Fig. S5), implying that disturbances in cell wall integrity might be due to defective glycosylation/mannosylation of cell wall components. Furthermore, the hypersensitivity of the mutant to SDS suggested a marked defect in cell membrane structure. Our results also demonstrated that the *pmi*-defi-

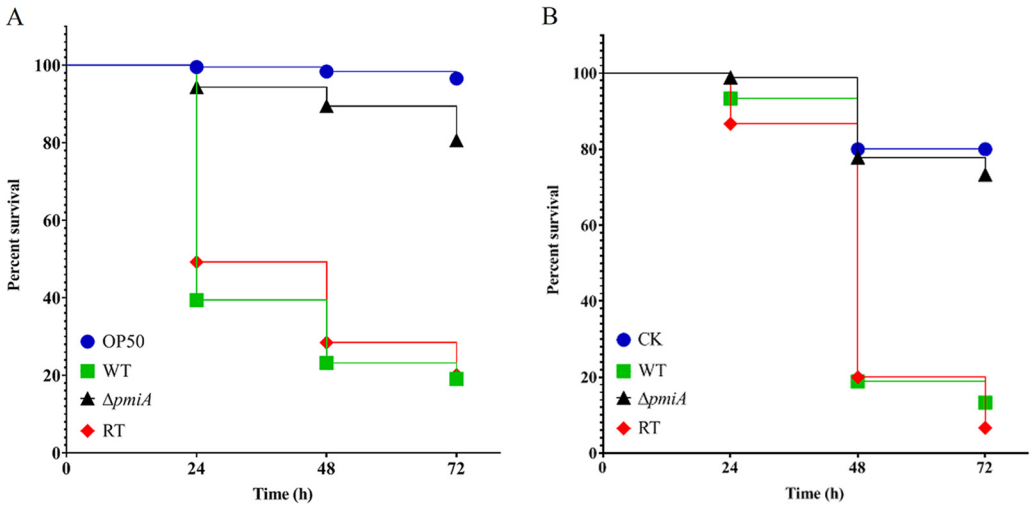

FIG 9 Virulence tests of *A. flavus* strains in *C. elegans* and *G. mellonella* models. (A) Kaplan-Meier survival plot of *glp-4* (bn2) and *sek-1* (km4) worms fed by the conidia of indicated strains after 16 h of infection. Worms infected with *Escherichia coli* OP50 strain were used as control. For each strain, three biological repeats (each with triplicates) were conducted. (B) Kaplan-Meier survival plot of *G. mellonella* larvae at 24, 48, and 72 h after infection with conidia of the indicated strain. Larvae treated with heat-killed spores were used as control (CK). The incubation temperature was 28°C. For each strain, three biological repeats (each with triplicates) were conducted.

cient strain did not develop sclerotia either at 28°C (Fig. 8) or 37°C (Fig. 4), which are repositories for the production of sexual spores in harsh and stress conditions (24). This might be the reason for the reduced tolerance of the mutant toward stresses, including SDS, H_2O_2, and osmotic stabilizers (Fig. 5).

Infection of plants by pathogenic fungi is a complex process (45). Our results from the infection assays demonstrated that the Δ*pmiA* mutant was unable to colonize and grow on corn and peanut seeds (Fig. 6A to C) and thus was unable to produce AFB1 (Fig. 7). Similarly, the *pmi*-deficient strain was inefficient in causing virulence in *C. elegans* and *G. mellonella* models (Fig. 9). All these results imply that *A. flavus* PMI has a critical role in triggering virulence in animals and plants.

In conclusion, our study here fully characterized the function of PMI in *A. flavus*, revealing that PMI in *A. flavus* is essential for growth, conidiation, stress responses, and pathogenicity in both plant and animal models. Despite that developing an inhibitor selectively targeting *A. flavus* PMI but not a human PMI orthologue is far away, newly rising approaches, such as fragment-based drug discovery, will facilitate the exploration of selective inhibitors against highly conserved potent targets (46). Nonconserved sites of the target could be explored for selectivity, such as the selective inhibitors against *Plasmodium falciparum N*-myristoyltransferase (NMT) that were developed based only on the single-residue difference from human orthologue (47, 48). Recently, we also confirmed that *A. fumigatus* phosphoglucose isomerase (PGI) possesses an exploitable site and space for developing selective inhibitors (49). Applying PMI inhibitors in the agricultural field will be more reachable since the PMIs are less ubiquitous in the kingdom Plantae and are reported absent in many plants (27). Therefore, PMI could be a promising target to battle against infection and control crop contaminations caused by *A. flavus*.

MATERIALS AND METHODS

Fungal strains, media, and culture conditions. The uracil auxotroph strain CA14Δ*ku70*Δ*pyrG* was used as the parental strain for transformation, and CA14Δ*ku70* was used as the wild-type (WT) strain for phenotypic analysis. All strains were cultured at 37°C or 28°C and stored at 4°C for the short term and at −80°C in glycerol stocks for the long term. MM medium was used for the WT and revertant strains. MM supplemented with 5 mM uracil and uridine or with 3 mM mannose was used for the *pyrG* auxotroph and mutant strains, respectively. The primers used in the study are listed in Table S1 in the supplemental material.

Phylogenetic analysis. The PMI sequence for *A. flavus* was downloaded after a tBLASTn search of the genome using the *A. fumigatus* PMI sequence. PMI sequences from *Aspergillus caelatus*, *Aspergillus candidus*, *Saccharomyces cerevisiae*, *Aspergillus pseudotamarii*, *Aspergillus pseudonomiae*, *Aspergillus bombycis*, *Aspergillus nomius*, *Aspergillus oryzae*, *Aspergillus fumigatus*, *Fusarium oxysporum*, and *Candida albicans* were obtained from the National Center of Biotechnological Information (NCBI). The phylogenetic tree was produced using the neighbor-joining method and bootstrap test of 1,000 replicates in MEGA 5.0 software (50).

Construction of mutant and revertant strains. The mutant and revertant strains were constructed by homologous recombination strategy. Upstream and downstream flanking regions of 1.5 kb each from CA14Δ*ku70* and *A. fumigatus pyrG* selectable marker from the *AfpyrG* plasmid were PCR amplified using PrimeStar HS TaKaRa Taq mix (code no. R010Q). The three fragments were assembled in pCE zero vector using the seamless cloning kit (Vazyme, China). Then, the fused fragment, *up-pyrG-down*, was amplified from the vector and transformed into the CA14Δ*ku70*Δ*pyrG* protoplast to generate the Δ*pmiA* mutants by screening on MM medium supplemented with mannose. The revertant strain (RT) was constructed according to the method previously described (51). In the first round, the 4.5-kb flanking region from upstream to downstream of the WT genomic DNA was amplified and transformed into mutant protoplasts to screen *pyrG* auxotrophic strains on transforming plates without mannose supplementation. In the second round, the *pyrG* marker was inserted between the gene and downstream region and transformed to the screened *pyrG* auxotrophic protoplasts. All the strains were confirmed by PCR using four pairs of primers to ensure homologous recombination.

Effect of exogenous mannose on the strains. To optimize the growth condition of the mutant, MM plates with different concentrations of mannose (0, 0.5, 3, 5, 10, and 25 mM) were prepared. Serially diluted conidia (10^6 to 10^3) from WT, Δ*pmiA*, and RT strains were spotted on these plates and were incubated at 37°C for 2 days.

Growth phenotype, conidia production, and sclerotium formation analysis. To test the growth rate on solid plates, 10^6 conidia from the WT, Δ*pmiA*, and RT strains were inoculated onto the center of MMM solid medium plates for incubation at 37°C or 28°C. Colony diameters for each strain were recorded every 24 h along the same line for 10 days. Colony morphologies were photographed on the 3rd and 9th days of inoculation, and growth curves were drawn after 10 days. Conidia were collected by washing with 0.2% (vol/vol) Tween 20 and were counted by hemocytometer.

To analyze sclerotia production, 10^6 conidia from the WT, Δ*pmiA*, and RT strains were inoculated onto the center of sclerotial induction medium YPD containing 1% glucose and 3 mM mannose as carbon sources. Plates were incubated at 37°C in the dark to induce sclerotia. Colony morphology was photographed under a

microscope after 10 days of incubation. The mycelia and spores on the plates were washed out with 75% alcohol, and the colony morphology was again photographed under a microscope. In addition, the sclerotia production of WT and RT strains at 28°C was performed on 1% peanut powder plates. Sclerotia formation of the Δ*pmiA* mutant at 28°C was conducted on MMM supplemented with 1% peanut powder.

To observe the morphology of conidiophores, a small steel ring with holes was fixed between a slide and a coverslip with wax solution. The holes were sealed with wax by injecting molten MMM medium into the ring. Conidia from WT, Δ*pmiA*, and RT strains were inoculated to the solidified medium by a fine wire dip. The samples were incubated at 37°C in the upright position and were examined every 24 h. When conidiophore growth was observed, a solution of lactic acid phenol cotton blue dye was added on the conidiophore cluster with a syringe, and photos were taken under a microscope.

Hyphal morphology and germination statistics. Spore germination experiments were performed in 96-well plates. Conidia of 10^5 were inoculated into 200 μL MMM liquid medium and incubated at 37°C. The spore germination status was observed under a microscope after 6 h, 8 h, and 10 h of incubation. The hyphal morphology was randomly photographed, and over 100 cells of each strain were selected to count the germination rate. The mycelial morphology of the mutant was also observed under different mannose concentrations (0.5, 3, 5, 10, 25, and 40 mM) and was photographed at 10 h and 48 h.

Assays for sensitivity to stress and temperature conditions. Stresses, including Congo red (CR), calcofluor white (CFW), sodium dodecyl sulfate (SDS), sodium chloride (NaCl), potassium chloride (KCl), sorbitol, and hydrogen peroxide (H_2O_2), were conducted. Briefly, serially diluted conidia (10^6 to 10^3) from the WT, Δ*pmiA*, and RT strains were point inoculated on MMM plates containing the mentioned stress chemicals at different concentrations and incubated at 37°C.

Cell wall content analysis. The cell wall components were determined using the previously described method (25). Briefly, 10^7 conidia of the WT, Δ*pmiA*, and RT strains were inoculated into MMM liquid medium and cultured at 37°C, 200 rpm. After 48 h, mycelia were harvested by filtration and were converted to fine powder by grinding in liquid nitrogen. SDS-BME [50 mM Tris, 50 mM EDTA, 2% SDS, and 1 mM Tris(2-carboxyethyl)phosphine hydrochloride (TCEP)] was added to the powder and boiled at 100°C for 40 min. After centrifugation, cell wall fractions were thoroughly washed with Milli-Q water and were freeze-dried for 3 days. We added 75 μL of 72% H_2SO_4 to 10 mg cell dry mass and left for 3 h at room temperature. The pellet was then resuspended in 0.95 mL Milli-Q water and boiled at 100°C for 4 h. After neutralization to pH 7 by $Ba(OH)_2$, the samples were left at 4°C overnight. The monosaccharide content in the supernatant was determined by high-performance anion-exchange chromatography coupled with a pulsed amperometric detector (HPAEC-PAD) using a CarboPac PA-10 anion exchange column equipped with an Amino trap guard column at room temperature. Elution was performed at a flow rate of 1 mL min^{-1} using 18 mM NaOH at room temperature.

Peanut and corn seed infection. Fresh peanut and corn seeds of similar size and shape were selected and washed with 0.05% sodium hypochlorite for 3 min and then 75% ethanol for 1 min. To avoid germination, the endosperm was removed by toothpicks. The seeds were then washed three times with sterile water; inoculated with 10^6 conidia of WT, Δ*pmiA*, and RT strains; and incubated at 28°C for 6 days in the dark. During the incubation period, the humid conditions for seeds were maintained by using wet filter paper. After incubation, the infected seeds were transferred to 20 mL of 0.2% Tween 20 in 50-mL tubes. The tubes were shaken at 200 rpm for 5 min, and the conidia were released. One-milliliter aliquots of conidia were taken from each sample, serially diluted, and counted using a hemocytometer. To check the growth ability of the mutant under a natural nutritional environment, peanut and corn seeds were ground to powder form. Concentrations of 1%, 3%, and 5% (wt/vol) corn and peanut powder were mixed with agar to prepare solid plates. Fresh conidia ($10^{5)}$ of the WT, Δ*pmiA*, and RT strains were inoculated in the center of the plates and incubated at 37°C for 6 days. In addition, the mycelium slices of the WT, Δ*pmiA*, and RT strains were placed onto the center of the above-mentioned peanut and corn plates and cultured at 28°C.

TLC and detection of AFB1. Using an equal volume of chloroform, aflatoxin was extracted from 500 μL of filtrate, and the chloroform layer was transferred to a fresh tube, which was then dried at 70°C. Aflatoxin production was detected by TLC using a solvent system of chloroform/acetone at 9:1 and visualized under UV at 365 nm wavelength.

Virulence studies in animal models. In accordance with an established virulence test using the *Caenorhabditis elegans*-based infection model (28), we tested the pathogenicity of the WT, Δ*pmiA*, and RT strains. Briefly, worms were infected with 10^8 conidia of the fungal strains at 25°C. After 16 h, the pre-infected worms were transferred to killing assay medium (brain heart infusion [BHI+]) at 20°C. Survival rates of worms at 24 h, 48 h, and 72 h postinfection were recorded. The hyphal filamentation rate represents the rate of hyphal filaments that protruded from worm bodies.

For virulence test in *Galleria mellonella*, six instar larvae were selected and divided into 4 groups, each containing 90 larvae. Conidia of 10^4 from WT, Δ*pmiA*, and RT strains were injected into the hind proleg of larvae by Hamilton syringe. Larvae treated with heat-killed spores were used as a control (CK). After infection, the larvae were incubated at 28°C, and the survival rate was recorded for each group at 24 h, 48 h, and 72 h. Larvae that had apparent melanization or dark spots and were unable to move were considered dead.

Statistical analysis. GraphPad Prism 8 software was used to plot all the curves in this study. All data were presented as mean ± standard deviation (SD). The comparative analysis of statistical significance was done by one-way analysis of variance (ANOVA) for multiple-comparison analysis.

SUPPLEMENTAL MATERIAL

Supplemental material is available online only.

SUPPLEMENTAL FILE 1, PDF file, 1.3 MB.

ACKNOWLEDGMENTS

W.F. and C.J. conceived the study. S.U. performed genetic experiments. C.D. performed cell wall content analysis and larvae pathogenicity tests. A.S.O. executed the nematode pathogenicity tests. S.U., C.D., W.F., and C.J. analyzed and interpreted the data and wrote the manuscript with input from all authors. All authors have read and agreed to the final manuscript.

This work was supported by the National Natural Science Foundation of China (31960032, 32071279) and Guangxi Natural Science Foundation (2020GXNSFDA238008) to W.F.

We declare no conflict of interest.

REFERENCES

1. Skerker JM, Pianalto KM, Mondo SJ, Yang K, Arkin AP, Keller NP, Grigoriev IV, Louise Glass NL. 2021. Chromosome assembled and annotated genome sequence of Aspergillus flavus NRRL 3357. G3 (Bethesda) 11: jkab213. https://doi.org/10.1093/g3journal/jkab213.
2. Rudramurthy SM, Paul RA, Chakrabarti A, Mouton JW, Meis JF. 2019. Invasive aspergillosis by Aspergillus flavus: epidemiology, diagnosis, antifungal resistance, and management. J Fungi (Basel) 5:55. https://doi.org/10.3390/jof5030055.
3. Fernandez NB, Caceres DH, Beer KD, Irrazabal C, Delgado G, Farias L, Chiller TM, Verweij PE, Stecher D. 2021. Ventilator-associated pneumonia involving Aspergillus flavus in a patient with coronavirus disease 2019 (COVID-19) from Argentina. Med Mycol Case Rep 31:19–23. https://doi.org/10.1016/j.mmcr.2020.07.001.
4. Jasim NO, Klaaf M. 2021. Pulmonary aspergillosis associated with COVID-19. Int J Drug Deliv Technol 11:892–895.
5. Amaike S, Keller NP. 2011. Aspergillus flavus. Annu Rev Phytopathol 49: 107–133. https://doi.org/10.1146/annurev-phyto-072910-095221.
6. Klich MA. 2007. Aspergillus flavus: the major producer of aflatoxin. Mol Plant Pathol 8:713–722. https://doi.org/10.1111/j.1364-3703.2007.00436.x.
7. Muszewska A, Piłsyk S, Perlińska-Lenart U, Kruszewska J. 2017. Diversity of cell wall related proteins in human pathogenic fungi. J Fungi (Basel) 4:6. https://doi.org/10.3390/jof4010006.
8. Chow J, Notaro M, Prabhakar A, Free S, Cullen P. 2018. Impact of fungal MAPK pathway targets on the cell wall. J Fungi (Basel) 4:93. https://doi.org/10.3390/jof4030093.
9. Hopke A, Brown AJP, Hall RA, Wheeler RT. 2018. Dynamic fungal cell wall architecture in stress adaptation and immune evasion. Trends Microbiol 26:284–295. https://doi.org/10.1016/j.tim.2018.01.007.
10. Lima SL, Colombo AL, de Almeida Junior JN. 2019. Fungal cell wall: emerging antifungals and drug resistance. Front Microbiol 10:2573. https://doi.org/10.3389/fmicb.2019.02573.
11. Hasim S, Coleman JJ. 2019. Targeting the fungal cell wall: current therapies and implications for development of alternative antifungal agents. Future Med Chem 11:869–883. https://doi.org/10.4155/fmc-2018-0465.
12. Kang X, Kirui A, Muszyński A, Widanage MCD, Chen A, Azadi P, Wang P, Mentink-Vigier F, Wang T. 2018. Molecular architecture of fungal cell walls revealed by solid-state NMR. Nat Commun 9:2747. https://doi.org/10.1038/s41467-018-05199-0.
13. Engel J, Schmalhorst PS, Routier FH. 2012. Biosynthesis of the fungal cell wall polysaccharide galactomannan requires intraluminal GDP-mannose. J Biol Chem 287:44418–44424. https://doi.org/10.1074/jbc.M112.398321.
14. Lockhart DEA, Stanley M, Raimi OG, Robinson DA, Boldovjakova D, Squair DR, Ferenbach AT, Fang W, van Aalten DMF. 2020. Targeting a critical step in fungal hexosamine biosynthesis. J Biol Chem 295:8678–8691. https://doi.org/10.1074/jbc.RA120.012985.
15. Fang W, Du T, Raimi OG, Hurtado-Guerrero R, Mariño K, Ibrahim AFM, Albarbarawi O, Ferguson MAJ, Jin C, Van Aalten DMF. 2013. Genetic and structural validation of Aspergillus fumigatus N-acetylphosphoglucosamine mutase as an antifungal target. Bioscience Rep 33. https://doi.org/10.1042/BSR20130053.
16. Fang W, Du T, Raimi OG, Hurtado-Guerrero R, Urbaniak MD, Ibrahim AFM, Ferguson MAJ, Jin C, van Aalten DMF. 2013. Genetic and structural validation of A spergillus fumigatus UDP-N-acetylglucosamine pyrophosphorylase as an antifungal target. Mol Microbiol 89:479–493. https://doi.org/10.1111/mmi.12290.
17. Wills EA, Roberts IS, Del Poeta M, Rivera J, Casadevall A, Cox GM, Perfect JR. 2001. Identification and characterization of the Cryptococcus neoformans phosphomannose isomerase-encoding gene, MAN1, and its impact on pathogenicity. Mol Microbiol 40:610–620. https://doi.org/10.1046/j.1365-2958.2001.02401.x.
18. Barcelos MP, Federico LB, Taft CA, de Paula da Silva CHT. 2020. Prediction of the three-dimensional structure of phosphate-6-mannose PMI present in the cell membrane of Xanthomonas citri subsp. citri of interest for the citrus canker control, p 259–276. *In* La Porta F, Taft C (ed), Emerging research in science and engineering based on advanced experimental and computational strategies. Springer, Cham, Switzerland.
19. Bangera M, Gowda K G, Sagurthi SR, Murthy MRN. 2019. Structural and functional insights into phosphomannose isomerase: the role of zinc and catalytic residues. Acta Crystallogr D Struct Biol 75:475–487. https://doi.org/10.1107/S2059798319004169.
20. DeRossi C, Bode L, Eklund EA, Zhang F, Davis JA, Westphal V, Wang L, Borowsky AD, Freeze HH. 2006. Ablation of mouse phosphomannose isomerase (Mpi) causes mannose 6-phosphate accumulation, toxicity, and embryonic lethality. J Biol Chem 281:5916–5927. https://doi.org/10.1074/jbc.M511982200.
21. Fang W, Yu X, Wang B, Zhou H, Ouyang H, Ming J, Jin C. 2009. Characterization of the Aspergillus fumigatus phosphomannose isomerase Pmi1 and its impact on cell wall synthesis and morphogenesis. Microbiology (Reading) 155:3281–3293. https://doi.org/10.1099/mic.0.029975-0.
22. Garami A, Ilg T. 2001. The role of phosphomannose isomerase in Leishmania mexicana glycoconjugate synthesis and virulence. J Biol Chem 276: 6566–6575. https://doi.org/10.1074/jbc.M009226200.
23. Cao Y, Li M, Xia Y. 2011. Mapmi gene contributes to stress tolerance and virulence of the entomopathogenic fungus, Metarhizium acridum. J Invertebr Pathol 108:7–12. https://doi.org/10.1016/j.jip.2011.06.002.
24. Horn BW, Sorensen RB, Lamb MC, Sobolev VS, Olarte RA, Worthington CJ, Carbone I. 2014. Sexual reproduction in Aspergillus flavus sclerotia naturally produced in corn. Phytopathology 104:75–85. https://doi.org/10.1094/PHYTO-05-13-0129-R.
25. Francois JM. 2006. A simple method for quantitative determination of polysaccharides in fungal cell walls. Nat Protoc 1:2995–3000. https://doi.org/10.1038/nprot.2006.457.
26. Puttikamonkul S, Willger SD, Grahl N, Perfect JR, Movahed N, Bothner B, Park S, Paderu P, Perlin DS, Cramer RA. 2010. Trehalose 6-phosphate phosphatase is required for cell wall integrity and fungal virulence but not trehalose biosynthesis in the human fungal pathogen Aspergillus fumigatus. Mol Microbiol 77:891–911. https://doi.org/10.1111/j.1365-2958.2010.07254.x.
27. Wu H, Canton M, Mahmoud LM, Weber KR, Michalczyk GZ, Dutt M, Zale JM. 2022. Identification and characterization of two putative citrus phosphomannose isomerase (CsPMI) genes as selectable markers for mature citrus transformation. Horticulturae 8:204. https://doi.org/10.3390/horticulturae8030204.
28. Ahamefule CS, Qin Q, Odiba AS, Li S, Moneke AN, Ogbonna JC, Jin C, Wang B, Fang W. 2020. Caenorhabditis elegans-based Aspergillus fumigatus infection model for evaluating pathogenicity and drug efficacy. Front Cell Infect Microbiol 10:320. https://doi.org/10.3389/fcimb.2020.00320.
29. Pukkila-Worley R, Peleg AY, Tampakakis E, Mylonakis E. 2009. Candida albicans hyphal formation and virulence assessed using a Caenorhabditis elegans infection model. Eukaryot Cell 8:1750–1758. https://doi.org/10.1128/EC.00163-09.
30. Brauer VS. 2020. Ação imunomoduladora de vesículas extracelulares produzidas por Aspergillus flavus. Universidade de São Paulo, São Paulo, Brazil.
31. Picot A, Ortega-Beltran A, Puckett RD, Siegel JP, Michailides TJ. 2017. Period of susceptibility of almonds to aflatoxin contamination during development in the orchard. Eur J Plant Pathol 148:521–531. https://doi.org/10.1007/s10658-016-1108-2.
32. Kachapulula PW, Akello J, Bandyopadhyay R, Cotty PJ. 2017. Aflatoxin contamination of groundnut and maize in Zambia: observed and potential concentrations. J Appl Microbiol 122:1471–1482. https://doi.org/10.1111/jam.13448.

33. Essono G, Ayodele M, Akoa A, Foko J, Filtenborg O, Olembo S. 2009. Aflatoxin-producing Aspergillus spp. aflatoxin levels in stored cassava chips as affected by processing practices. Food Control 20:648–654. https://doi.org/10.1016/j.foodcont.2008.09.018.
34. Fouad A, Ruan D, El-Senousey H, Chen W, Jiang S, Zheng C. 2019. Harmful effects and control strategies of aflatoxin B1 produced by Aspergillus flavus and Aspergillus parasiticus strains on poultry. Toxins 11:176. https://doi.org/10.3390/toxins11030176.
35. Joshi P, Maneeboon T, Cheerakupt C. 2021. Mycotoxins in foods: occurrence, challenges and management in context of Nepal. Int J Appl Sci Biotechnol 9:152–159. https://doi.org/10.3126/ijasbt.v9i3.38758.
36. Cortés JCG, Curto MÁ, Carvalho VSD, Pérez P, Ribas JC. 2019. The fungal cell wall as a target for the development of new antifungal therapies. Biotechnol Adv 37:107352. https://doi.org/10.1016/j.biotechadv.2019.02.008.
37. Ibe C, Oladele RO, Alamir O. 2022. Our pursuit for effective antifungal agents targeting fungal cell wall components: where are we? Int J Antimicrobial Agents 59:106477. https://doi.org/10.1016/j.ijantimicag.2021.106477.
38. Liu W, Yuan L, Wang S. 2020. Recent progress in the discovery of antifungal agents targeting the cell wall. J Med Chem 63:12429–12459. https://doi.org/10.1021/acs.jmedchem.0c00748.
39. Espitia C, Servín-González L, Mancilla R. 2010. New insights into protein O-mannosylation in actinomycetes. Mol Biosyst 6:775–781. https://doi.org/10.1039/b916394h.
40. de la Fuente M, Penas PF, Sols A. 1986. Mechanism of mannose toxicity. Biochem Biophys Res Commun 140:51–55. https://doi.org/10.1016/0006-291X(86)91056-9.
41. Adnan M, Zheng W, Islam W, Arif M, Abubakar Y, Wang Z, Lu G. 2017. Carbon catabolite repression in filamentous fungi. Int J Mol Sci 19:48. https://doi.org/10.3390/ijms19010048.
42. Zhang Y, Fang W, Raimi OG, Lockhart DEA, Ferenbach AT, Lu L, van Aalten DMF. 2021. Genetic and structural validation of phosphomannomutase as a cell wall target in Aspergillus fumigatus. Mol Microbiol 116:245–259. https://doi.org/10.1111/mmi.14706.
43. Jiang H, Ouyang H, Zhou H, Jin C. 2008. GDP-mannose pyrophosphorylase is essential for cell wall integrity, morphogenesis and viability of Aspergillus fumigatus. Microbiology (Reading) 154:2730–2739. https://doi.org/10.1099/mic.0.2008/019240-0.
44. Smith DJ, Payton MA. 1994. Hyphal tip extension in Aspergillus nidulans requires the manA gene, which encodes phosphomannose isomerase. Mol Cell Biol 14:6030–6038. https://doi.org/10.1128/mcb.14.9.6030-6038.1994.
45. Geoghegan I, Steinberg G, Gurr S. 2017. The role of the fungal cell wall in the infection of plants. Trends Microbiol 25:957–967. https://doi.org/10.1016/j.tim.2017.05.015.
46. Scott DE, Coyne AG, Hudson SA, Abell C. 2012. Fragment-based approaches in drug discovery and chemical biology. Biochemistry 51:4990–5003. https://doi.org/10.1021/bi3005126.
47. Bell AS, Mills JE, Williams GP, Brannigan JA, Wilkinson AJ, Parkinson T, Leatherbarrow RJ, Tate EW, Holder AA, Smith DF. 2012. Selective inhibitors of protozoan protein N-myristoyltransferases as starting points for tropical disease medicinal chemistry programs. PLoS Negl Trop Dis 6:e1625. https://doi.org/10.1371/journal.pntd.0001625.
48. Rackham MD, Brannigan JA, Rangachari K, Meister S, Wilkinson AJ, Holder AA, Leatherbarrow RJ, Tate EW. 2014. Design and synthesis of high affinity inhibitors of Plasmodium falciparum and Plasmodium vivax N-myristoyltransferases directed by ligand efficiency dependent lipophilicity (LELP). J Med Chem 57:2773–2788. https://doi.org/10.1021/jm500066b.
49. Zhou Y, Yan K, Qin Q, Raimi OG, Du C, Wang B, Ahamefule CS, Kowalski B, Jin C, van Aalten DMF, Fang W. 2022. Phosphoglucose isomerase is important for Aspergillus fumigatus cell wall biogenesis. mBio e01426-22. https://doi.org/10.1128/mbio.01426-22.
50. Hall BG. 2013. Building phylogenetic trees from molecular data with MEGA. Mol Biol Evol 30:1229–1235. https://doi.org/10.1093/molbev/mst012.
51. Zhou Y, Du C, Odiba AS, He R, Ahamefule CS, Wang B, Jin C, Fang W. 2021. Phosphoglucose isomerase plays a key role in sugar homeostasis, stress response, and pathogenicity in Aspergillus flavus. Front Cell Infect Microbiol 11:777266. https://doi.org/10.3389/fcimb.2021.777266.